Hindawi
Shock and Vibration
Volume 2024, Article ID 2628637, 12 pages
https://doi.org/10.1155/2024/2628637

Research Article

Research on Vehicle Vibration Fatigue Damage Potential under Non-Gaussian Road Profile Excitation

Fei Xu,[1] **Zhifeng Chen**,[1] **and Kjell Ahlin**[2]

[1]*School of Automotive Engineering, Yancheng Institute of Technology, Yancheng 224051, China*
[2]*Xielalin Consulting, S. Skogrundan 38, Akersberga SE-18463, Sweden*

Correspondence should be addressed to Fei Xu; luoyefeihen@163.com

Received 20 December 2023; Revised 27 February 2024; Accepted 13 March 2024; Published 21 March 2024

Academic Editor: Edoardo Sabbioni

The amplitude modulation method was used to generate a non-Gaussian road profile with prescribed power spectral density (PSD) and kurtosis. The vehicle vibration fatigue damage potential has been proven to be closely related to the amplitude modulation signal (AMS) and kurtosis of vehicle response. In this paper, the iterative method of AMS modelling based on absolute standard Gaussian distribution is first reviewed. To address the long iteration time problem, a closed-form formulation is presented to construct the AMS directly. Furthermore, by proving that the vehicle response under a slowly varying non-Gaussian road profile excitation can be regarded as the product of the same AMS and vehicle response under a Gaussian road profile excitation with the same PSD, the theoretical relationship between fatigue damage spectrum (FDS) of vehicle response under non-Gaussian and corresponding Gaussian road profiles is formulated based on the AMS. A case study is used to verify the proposed approach. The results show that a wide range of specified kurtosis of road profile can be achieved and the kurtosis of vehicle response is the same as for the road profile. Given kurtosis and fatigue exponent, the extra fatigue damage caused by non-Gaussian road profile can be derived easily from the corresponding Gaussian road profile without calculating the vehicle response, which lays the foundation for a significantly simplified and more accurate fatigue test of vehicle vibration under non-Gaussian road profile.

1. Introduction

A vibration test is often performed on vehicles in order to achieve comfort, durability, and safety requirements. As a major source of vehicle vibration and fatigue damage, road surface roughness is usually described by a Gaussian road profile and characterized by power spectral density (PSD) [1].

For a linear vehicle system, the vibration response under a Gaussian road profile excitation still follows a Gaussian distribution [2]. In practice, however, it has been found that the probability density function (PDF) of a typical road profile topography tends to be non-Gaussian and that the vehicle response tends to be significantly nonstationary and non-Gaussian due to the variations in road surface roughness and vehicle speed [3–5]. To evaluate the non-Gaussian response and fatigue damage, two types of non-Gaussian models were proposed: stationary non-Gaussian with peaks and nonstationary non-Gaussian with bursts. A comprehensive review of the stationary non-Gaussian model with peaks was presented in the article [6].

The amplitude modulation method for generating nonstationary non-Gaussian signal with bursts was first developed by Smallwood [7]. The essential idea is to model the non-Gaussian signal by multiplying a stationary Gaussian signal with a slowly varying amplitude modulation signal (AMS) that is independent of the Gaussian signal. The kurtosis of the generated non-Gaussian signal was governed by the parameters of the AMS. Different methods were proposed to construct the AMS, including beta distribution [7], gamma distribution [8], and Weibull distribution [9]. Xu et al. [10] indicated that when modelling the AMS by the Weibull distribution, inappropriate determination of the number of bursts may lead to distortion of the original PSD.

Among these methods, absolute standard Gaussian distribution was used by Trapp et al. [11] to construct the AMS. A wide range of kurtosis was achieved with good accuracy at the cost of a long iteration time.

Using the aforementioned methods, an acceleration test can be conducted by increasing the kurtosis while maintaining the same PSD level. However, it has been proved that the high kurtosis of the excitation signal does not necessarily transfer to the system response [12]. Rizzi et al. [13] found that a stationary non-Gaussian excitation results in a Gaussian response in a linear dynamic system. In contrast, it has been shown that the high kurtosis of nonstationary non-Gaussian excitation is more easily transferred to the system response, resulting in higher fatigue damage [14]. Kihm et al. [15] revealed the relationship between kurtosis of system response and excitation. Using stationary and nonstationary excitation, Braccesi et al. [16] investigated the transfer of kurtosis to the system response. Signals with different nonstationarity indices were produced by Capponi et al. [17] to investigate their impacts on fatigue life. Lei et al. [18] established a mathematical model for the kurtosis transmission law after the decomposition of excitation and response signals. Cornelis et al. [19] simulated non-Gaussian random vibrations on a shaker and analyzed the transfer of the non-Gaussian characteristics of the excitation signal. Fatigue damage spectrum (FDS) was used to evaluate the fatigue damage.

In this paper, the iterative method proposed by Trapp et al. [11] is further developed, in which a closed-form formulation is presented to construct the AMS. Based on the AMS, the theoretical relationship between FDS of vehicle response under non-Gaussian and corresponding Gaussian road profiles is formulated, which can be used to evaluate the extra fatigue damage caused by non-Gaussian road profile directly from corresponding Gaussian road profile without calculating the vehicle response.

The rest of the paper is organized as follows. In Section 2, Gaussian and non-Gaussian road profiles, the quarter car model, and the computation of FDS are presented. In Section 3, a closed-form formulation is presented to construct the AMS. Under the non-Gaussian road profile excitation, the theoretical relationship between FDS, kurtosis, and fatigue exponent is presented. In Section 4, a case study is used to verify the proposed approach. Finally, the conclusions are presented in Section 5.

2. Theoretical Background

2.1. Gaussian and Non-Gaussian Road Profile. A road profile $z(x)$ describes the road roughness as a function of distance. Gaussian road profiles are commonly used as models for road roughness, which can be characterized by a PSD [1].

$$G(\Omega) = G_0 \cdot \left(\frac{\Omega}{\Omega_0}\right)^{-w}, \tag{1}$$

where Ω is the spatial angular frequency, Ω_0 is the reference spatial angular frequency and $\Omega_0 = 1$ rad/m, G_0 is the roughness coefficient, $G_0 = 1.e^{-6}$ is a typical value, w is the slope of PSD on a loglog scale, and a typical value is $w = 2$.

Typical Gaussian and non-Gaussian road profiles are shown in Figure 1.

The PDF of a Gaussian road profile with zero mean value is expressed as follows:

$$p(z) = \frac{1}{\sqrt{2\pi}\sigma_z} e^{-\left(z^2/2\sigma_z^2\right)}, \tag{2}$$

where σ_z is the standard deviation.

$$\begin{aligned} \sigma_z^2 &= \mathrm{E}\left[z^2(x)\right], \\ &= \int_{-\infty}^{\infty} z^2 p(z)\mathrm{d}z, \end{aligned} \tag{3}$$

where $E[\ ]$ stands for expectation or mean value.

Kurtosis is used to identify whether a road profile is non-Gaussian:

$$K = \frac{M_4}{{\sigma_z}^4}, \tag{4}$$

where M_4 is the fourth-order central moment.

$$M_4 = E\left[(z(x) - \mu)^4\right], \tag{5}$$

where μ is the mean value.

A comparison of PDF of Gaussian (with kurtosis 3) and non-Gaussian (with kurtosis 6 and 9) road profiles is shown in Figure 2. From Figure 2, we can see that a kurtosis value greater than 3 indicates wider tails. A wider tail indicates a higher probability of larger peak values, which leads to larger fatigue damage and faster failure.

2.2. Quarter Car Modelling. A golden car model [20], as shown in Figure 3, is used to calculate the vehicle response. All parameters are normalized to m_s and shown in Table 1.

The motion equation of the golden car model can be written as follows:

$$\begin{bmatrix} m_s & 0 \\ 0 & m_u \end{bmatrix} \begin{Bmatrix} \ddot{z}_s(t) \\ \ddot{z}_u(t) \end{Bmatrix} + \begin{bmatrix} c_s & -c_s \\ -c_s & c_s \end{bmatrix} \begin{Bmatrix} \dot{z}_s(t) \\ \dot{z}_u(t) \end{Bmatrix} + \begin{bmatrix} k_s & -k_s \\ -k_s & k_s + k_t \end{bmatrix} \begin{Bmatrix} z_s(t) \\ z_u(t) \end{Bmatrix} = \begin{Bmatrix} 0 \\ k_t \cdot z(t) \end{Bmatrix}, \tag{6}$$

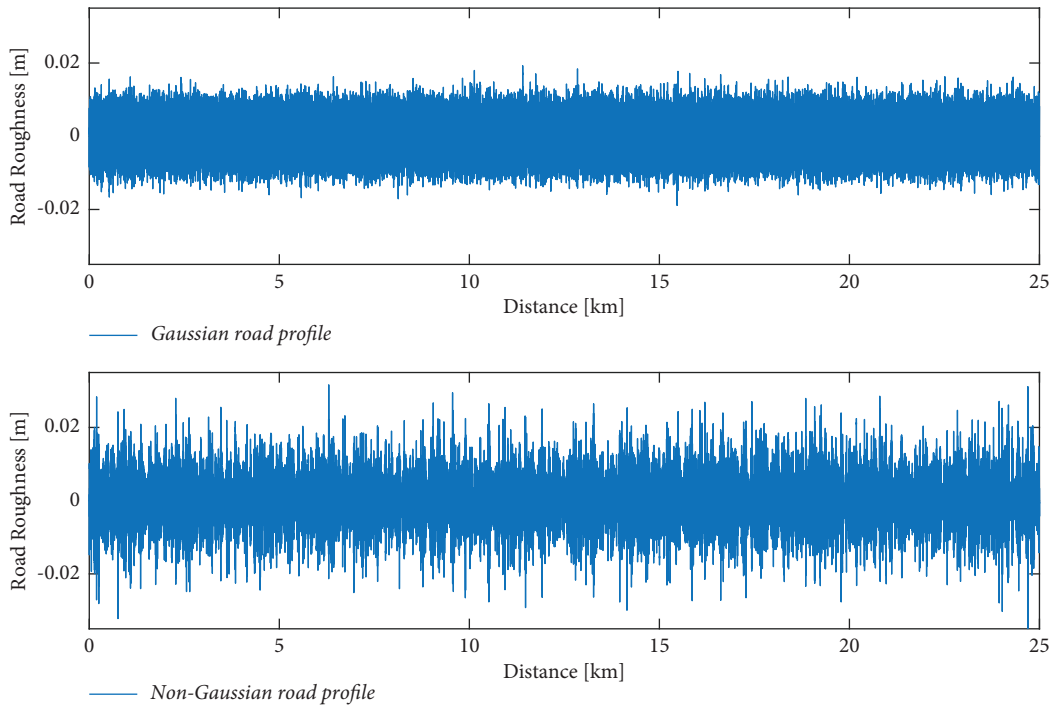

Figure 1: Typical Gaussian and non-Gaussian road profiles.

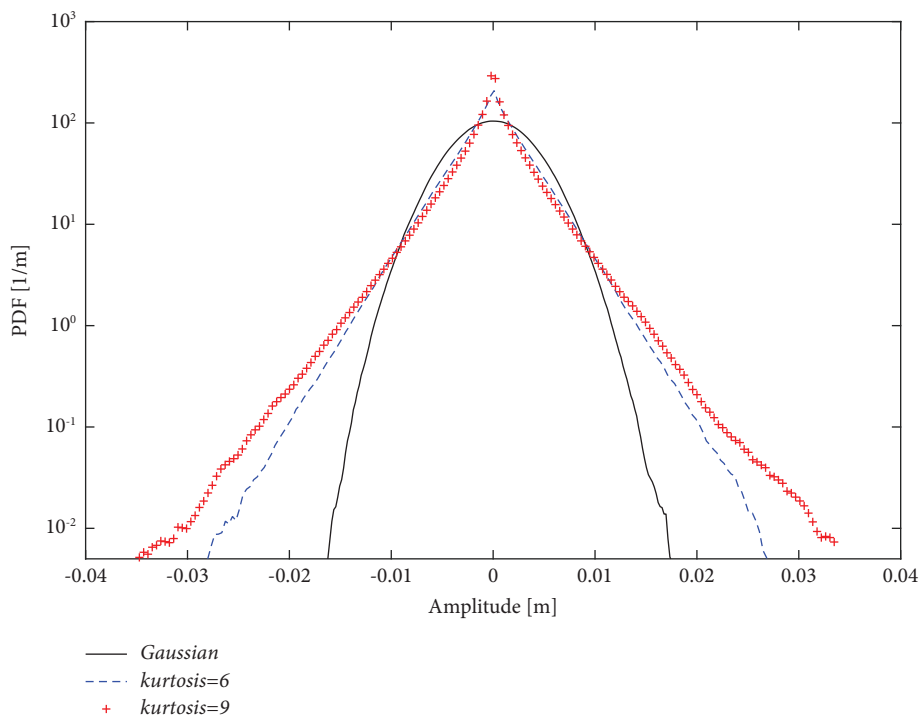

Figure 2: PDF comparison of road profiles with different kurtosis.

where $z_s(t)$ and $z_u(t)$ are the vertical displacements of sprung and unsprung mass, respectively, and $z(t)$ is the road profile in the time domain.

The ramp-invariant digital filter method [21] is used to calculate the vehicle response under road profile excitation. To transform the road profile from the spatial domain to the

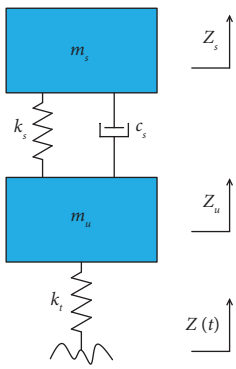

Figure 3: Golden car model.

Table 1: Golden car parameters.

Parameter	Unit	Value
m_s/m_s	Sprung mass (1)	1
m_u/m_s	Unsprung mass (1)	0.15
c_s/m_s	Suspension damping (s^{-1})	6
k_s/m_s	Suspension stiffness (s^{-2})	63.3
k_t/m_s	Tire stiffness (s^{-2})	653

time domain, a sampling frequency f_s in Hz can be calculated as follows:

$$f_s = \frac{v \cdot 1000}{3600} \cdot f_x = \frac{v}{3.6} \cdot f_x, \tag{7}$$

where v is the vehicle speed in km/h and f_x is the number of data samples per meter.

2.3. Fatigue Damage Spectrum (FDS). FDS is commonly used to evaluate the damage potential of non-Gaussian vibration. As shown in Figure 4, the FDS is calculated based on the responses of a series of single-degree-of-freedom (SDOF) systems to the same base excitation over a certain amount of time.

The stress is assumed to be proportional to pseudo-velocity [22]. The output pseudo-velocity (x_{pv}) to an input acceleration (x_a) for an SDOF system with a natural frequency (f_n) and a damping ratio (ξ) can be computed as follows:

$$x_{\text{pv}} = F_{\text{filter}}(b_n, a_n, x_a), \tag{8}$$

where F_{filter} indicates filtering of the input signal using a ramp-invariant digital filter. b_n and a_n are digital filter coefficients.

Using the output x_{pv}, the cumulative damage can be calculated in both time and frequency domains. In time domain, a faster algorithm than the rain flow cycle counting (RFCC) method [23] is used to calculate the total damage index D_t. It starts by converting the output pseudo-velocity into a peak-valley signal, where the data points between the maxima and minima are deleted. Each maximum $x_{\text{pv,pk},i}$ is regarded as the peak value of a cycle with the range $2x_{\text{pv,pk},i}$. The minima are counted in the same manner, and the sum is divided by 2.

$$\begin{aligned} D_t &= \sum_{i=1}^{q} \frac{|S_{pk,i}|^b}{2c}, \\ &= \sum_{i=1}^{q} \frac{k^b |x_{\text{pv,pk},i}|^b}{2c}, \end{aligned} \tag{9}$$

where $S_{\text{pk},i}$ ($i = 1, 2, \ldots, q$) is assumed to be proportional to the maximum and minimum values $x_{\text{pv,pk},i}$ and q is the number of maximum and minimum values considered, and b is the fatigue exponent in the S-N curve. According to [24], $c = k = 1$ is used in this study.

3. Fatigue Damage Based on a Novel AMS Modelling Method

3.1. A Novel AMS Modelling Method Using Closed-Form Formulation. The amplitude modulation method is used in this paper to model the non-Gaussian road profile:

$$z(x) = g(x) \cdot u(x), \tag{10}$$

where $g(x)$ is a Gaussian road profile generated from PSD and $u(x)$ is an independent slowly varying AMS.

To make the PSD of the non-Gaussian road profile approximately the same as that of the Gaussian road profile, the mean square of the AMS is scaled to 1. With equations (4) and (10), the kurtosis of $z(x)$ can be expressed as follows:

$$\begin{aligned} K_z &= \frac{E[z^4]}{E[z^2] \cdot E[z^2]}, \\ &= \frac{E[g^4 \cdot u^4]}{E[g^2 \cdot u^2] \cdot E[g^2 \cdot u^2]}, \\ &= \frac{E[g^4] \cdot E[u^4]}{E[g^2] \cdot E[g^2] \cdot E[u^2] \cdot E[u^2]}, \\ &= 3 \cdot \frac{E[u^4]}{E[u^2] E[u^2]}, \\ &= 3 \cdot K_u, \end{aligned} \tag{11}$$

where K_u is the kurtosis of AMS $u(x)$ with mean value.

Clearly, the kurtosis of $z(x)$ depends on K_u. So the crux of the method is the AMS modelling. To create the AMS, a slowly varying standard Gaussian signal $y(x)$ is first created and the absolute value is taken:

$$a(x) = |y(x)|. \tag{12}$$

To achieve target K_u, the AMS is modeled as follows:

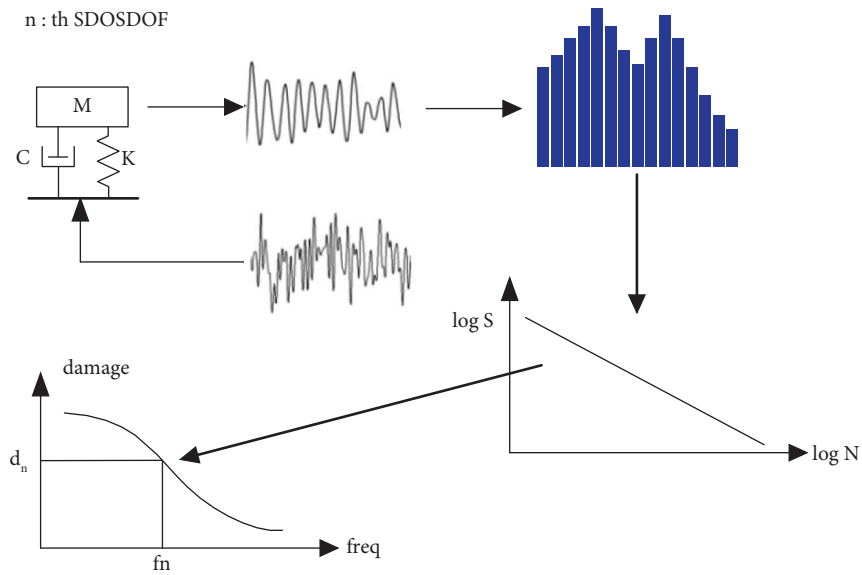

Figure 4: Calculation process of the FDS.

$$u(x) = |y(x)|^p, \\ = (a(x))^p. \tag{13}$$

Instead of iterating the exponent p until a desired K_u is generated, a closed-form formulation for the direct calculation of p is proposed. The m:th moment of $u(x)$ can be written as follows:

$$M_m[u(x)] = E[u(x)^m], \\ = \frac{E[(a(x))^{mp}]}{\{E[(a(x))^{2p}]\}^{(m/2)}}, \tag{14}$$

$$E[(a(x))^{mp}] = \frac{2}{\sqrt{2\pi}} \cdot \int_0^\infty x^{\mathrm{mp}} \cdot e^{-(x^2/2)} \mathrm{d}x, \tag{15}$$

$$E[(a(x))^{2p}] = \frac{2}{\sqrt{2\pi}} \cdot \int_0^\infty x^{2p} \cdot e^{-(x^2/2)} \mathrm{d}x. \tag{16}$$

Using the following equation,

$$\int_0^\infty x^p \cdot e^{-Ax^2} \mathrm{d}x = \frac{\Gamma(q+1/2)}{2\sqrt{A^{q+1}}}, \tag{17}$$

where Γ is the gamma function.

The general formula for the m:th moment of $u(x)$ is written as follows:

$$M_m(p) = \pi^{(m/4-1/2)} \cdot \frac{\Gamma(m \cdot \mathrm{p}/2 + 1/2)}{[\Gamma(p+1/2)]^{m/2}}. \tag{18}$$

The closed-form formulation between K_u and the p value can be derived when $m = 4$:

$$K_u = \pi^{0.5} \cdot \frac{\Gamma(4\mathrm{p}/2 + 1/2)}{[\Gamma(p+1/2)]^2}. \tag{19}$$

With given kurtosis of non-Gaussian road profile, the following equation can be solved in MATLAB to get p value:

$$s = \left[\frac{'\mathrm{gamma}(4 * x/2 + 1/2)}{(\mathrm{gamma}(x+1/2)) \wedge 2} - '\mathrm{num2str}\left(\frac{\mathrm{Ku}}{\mathrm{sqrt}(\mathrm{pi})}\right)\right], \tag{20}$$

$$p = \mathrm{fzero}(s, 1), \tag{21}$$

where * in MATLAB means multiplication.

The relationship between K_z and p in equation (21) was compared with the aforementioned iterative method as shown in Figure 5. As can be seen in Figure 5, a wide range of kurtosis can be generated and both methods give the same result. However, much higher efficiency can be achieved with the proposed closed-form formulation, since the p value can be calculated directly once the target kurtosis is determined.

3.2. Vehicle Response under Non-Gaussian Road Profile Excitation. Under the non-Gaussian road profile excitation, the response of m_s in Figure 3 can be calculated as follows:

$$r(t) = \{k_t \cdot z(t)\} * h(t), \\ = k_t \cdot \int_{t-T}^{t} u(\tau) \cdot g(\tau) \cdot h(t-\tau) \mathrm{d}\tau, \tag{22}$$

where $u(t)$ and $\mathrm{g}(t)$ are $u(x)$ and $\mathrm{g}(x)$ in equation (10) converted to time domain using f_s in equation (7), $h(t)$ is the impulse response function, T is the length of $h(t)$, and "*" denotes convolution here.

When the time domain AMS $u(t)$ is slowly varying, it can be regarded as a constant during T. Then, $u(t)$ can be taken outside the integral in equation (22), which indicates that the response under non-Gaussian road profile is the same as the response under Gaussian road profile, multiplied by the same AMS $u(t)$:

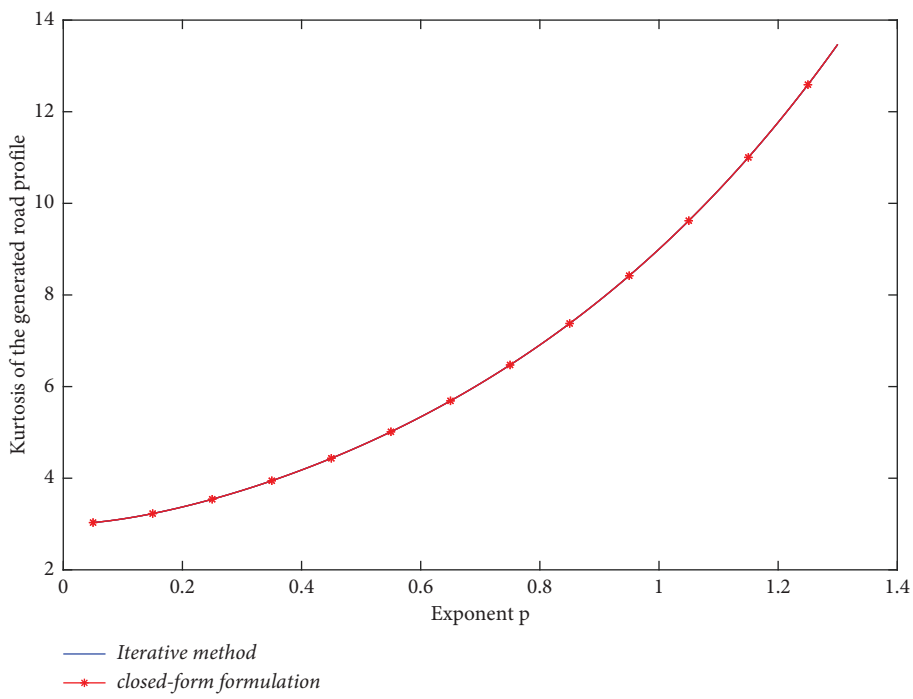

Figure 5: Comparison between closed-form formulation and iterative method.

$$r(t) = k_t \cdot u(t) \cdot \int_{t-T}^{t} g(\tau) \cdot h(t-\tau)\mathrm{d}\tau, \\ = u(t) \cdot k_t \cdot \{g(t) * h(t)\}. \tag{23}$$

A non-Gaussian road profile with PSD of ISO-A road surface (see Figure 6 in Chapter 3.2) and kurtosis 6 is used here as an example. The Gaussian road profile, AMS, and corresponding non-Gaussian road profile (converted into the time domain using $v = 70$ km/h) are shown in Figure 7. A comparison between vehicle responses under the non-Gaussian road profile excitation and under the Gaussian road profile excitation multiplied by $u(t)$ is shown in Figure 8. From Figure 8, we can see again that the vehicle response under non-Gaussian road profile is the same as the response under Gaussian road profile with the same PSD, multiplied by the same AMS $u(t)$.

3.3. Vehicle Fatigue Damage under Non-Gaussian Road Profile Excitation. Since the vehicle response is also a slowly varying non-Gaussian signal, the AMS $u(t)$ can be treated as a constant compared to the Gaussian part $g(t)$ for each specific time duration t_i. For each time duration, it is assumed that the value of AMS $u(t)$ is c_i and the proportion of this part in the entire time history is r_i. Using the time domain method, the damage for an SDOF system with natural frequency f_n $(n = 1, 2, \ldots)$ is as follows [23]:

$$D_z(t_i) = r_i c_i^b D_g(t_i), \tag{24}$$

where $D_g(t_i)$ is the fatigue damage caused by the Gaussian part in vehicle response.

The damage of the entire time history can be presented as follows:

$$D_z(T) = r_1 c_1^b D_g(t_1) + r_2 c_2^b D_g(t_2) + \cdots + r_n c_n^b D_g(t_n), \\ = D_g(T) \sum_{i=1}^{n} r_i c_i^b, \\ = D_g(T) \mathrm{E}\left[u(t)^b\right], \tag{25}$$

where n is the number of time sections.

If the AMS follows a certain distribution $f(u)$, then the damage can be expressed as follows:

$$|D_z(T) = \left[\int_0^T u^b \cdot f(u)\mathrm{d}u\right] \cdot \mathrm{D}_g(T). \tag{26}$$

The FDS ratio of vehicle response under non-Gaussian road profile excitation (denoted as $\mathrm{FDS_{NG}}$) to the one under Gaussian road profile excitation (denoted as $\mathrm{FDS_G}$) is $E(u(t)^b)$, which is denoted as *Quot* in this paper:

$$\mathrm{Quot} = \frac{\mathrm{FDS_{NG}}}{\mathrm{FDS_G}}, \\ = E\left[u(t)^b\right], \tag{27}$$

since

$$E\left[u(t)^b\right] = E\left[u(x)^b\right]. \tag{28}$$

Equation (18) can be used to express *Quot* as follows:

$$\mathrm{Quot} = \pi^{(b/4-1/2)} \cdot \frac{\Gamma(b(p/2) + 1/2)}{[\Gamma(p + 1/2)]^{b/2}}. \tag{29}$$

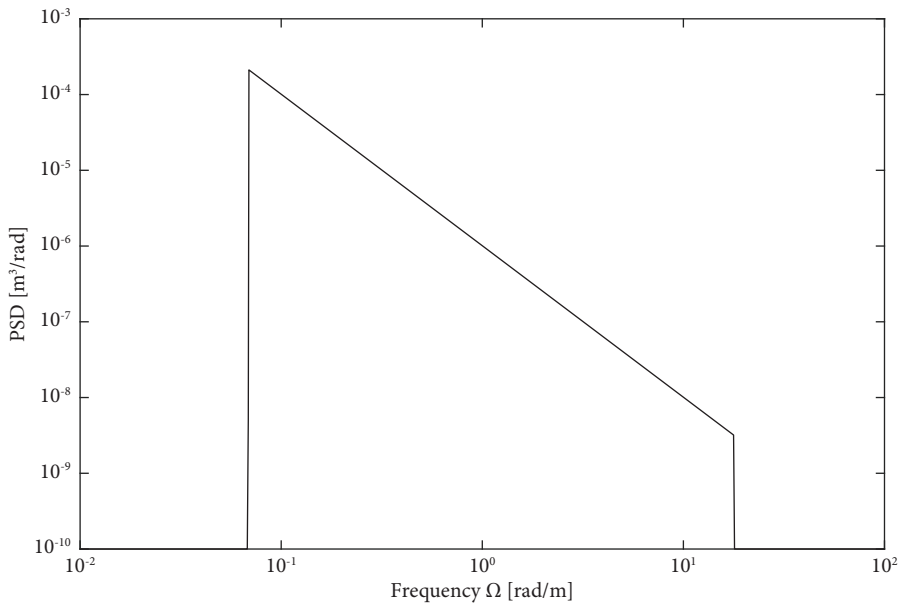

Figure 6: PSD of ISO-A road profile.

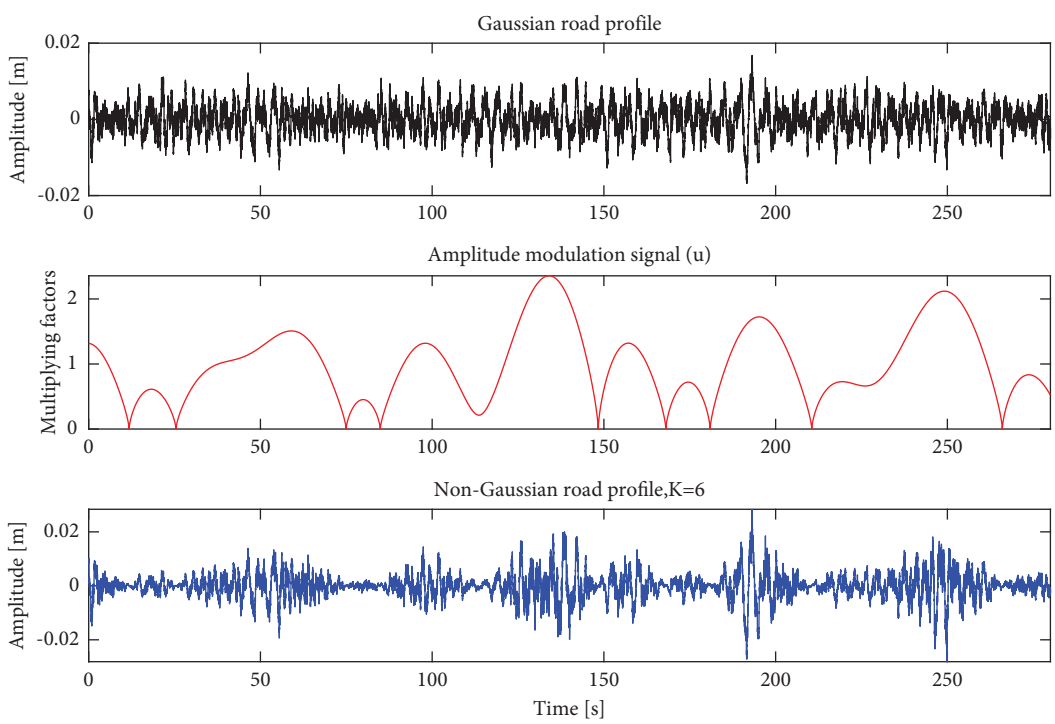

Figure 7: Gaussian road profile, AMS, and corresponding non-Gaussian road profile.

Given b and p calculated from equation (20) for a certain non-Gaussian road profile, equation (29) can be used to evaluate the extra fatigue damage caused by the non-Gaussian road profile excitation directly without calculating the vehicle response.

Another non-Gaussian road profile with PSD of ISO-A road surface and kurtosis 9 is used here as an example. The FDS of vehicle response under Gaussian and non-Gaussian road profile excitation is calculated. *Quot* is calculated using equation (29) with $b = 4$ and justified by a good match between FDS under non-Gaussian road profile and $Quot \times$ FDS under Gaussian road profile as shown in Figure 9.

4. Case Study

In the simulation process, the vehicle speed is assumed to be 70 km/h and the spatial angular frequency $f_z = 100 \times 2\pi$. The

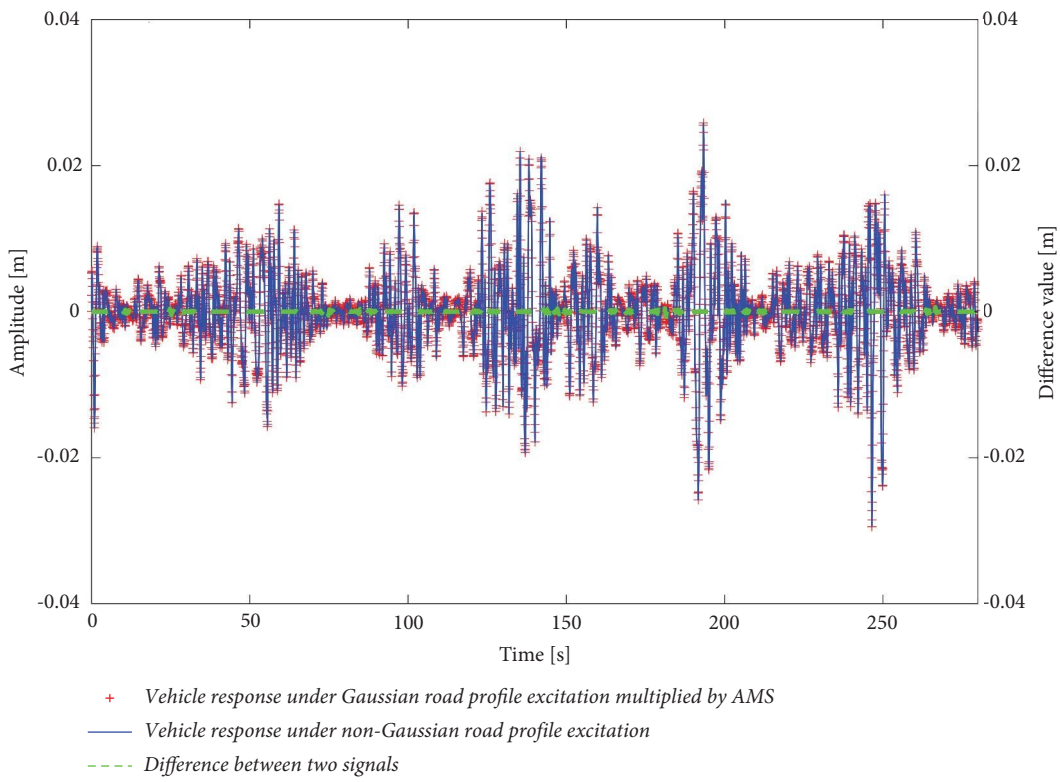

Figure 8: A comparison between vehicle responses under non-Gaussian road profile excitation and Gaussian road profile excitation multiplied by $u(t)$.

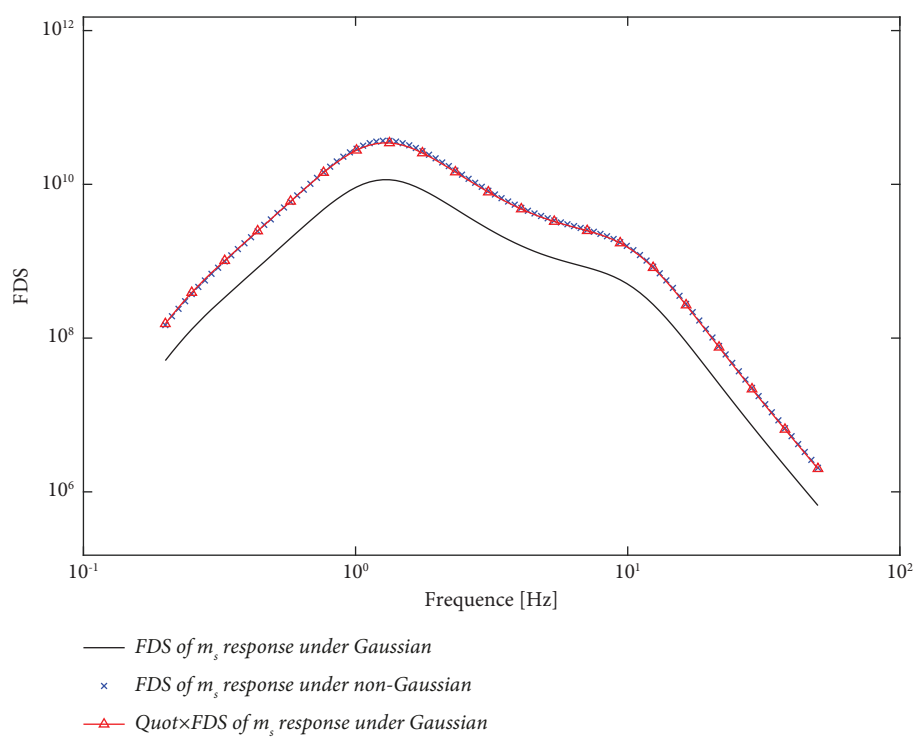

Figure 9: FDS of vehicle response under Gaussian and non-Gaussian road profile excitation.

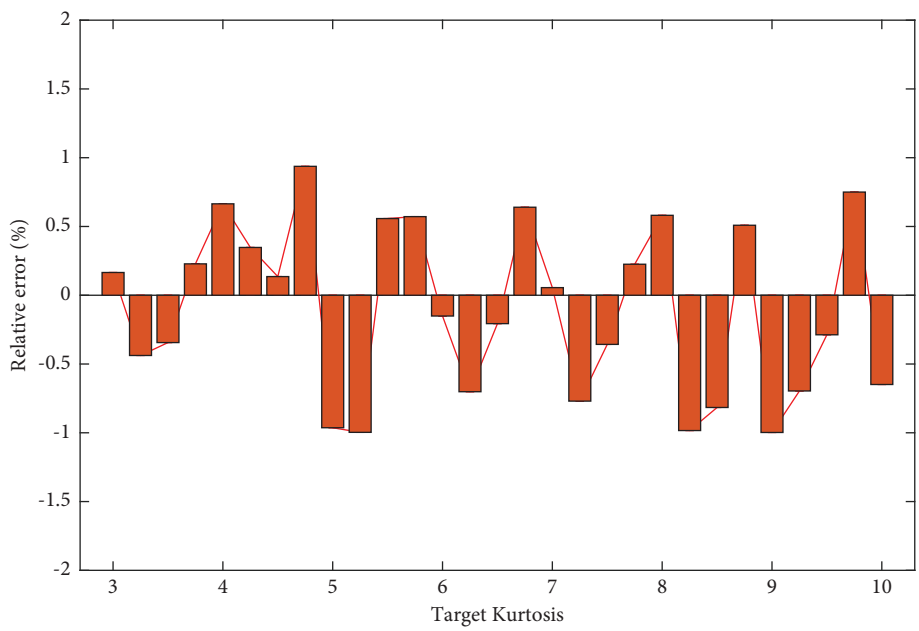

Figure 10: Relative error between target and generated kurtosis.

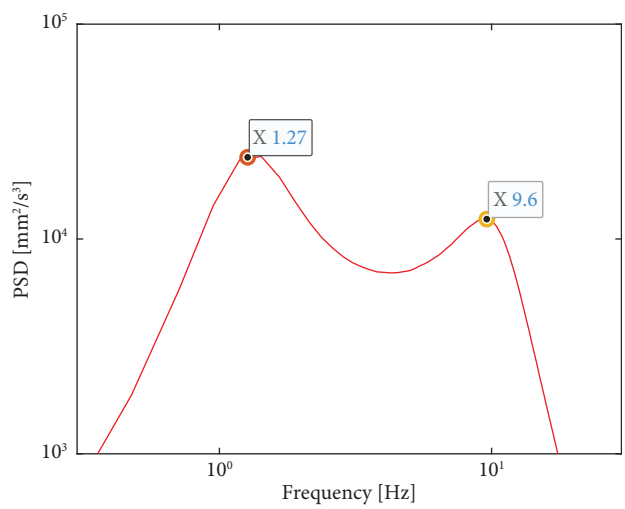

Figure 11: PSD of vehicle response at m_s.

ISO-8608 Class-A road profile is used in this case study. The PSD is shown in Figure 6. The spatial angular frequency is from $0.011 \times 2\pi$ to $2.83 \times 2\pi\, rad{\cdot}\mathrm{m}^{-1}$.

The relative error between target and generated kurtosis is shown in Figure 10. From Figure 10, we can see that a wide range of target kurtosis is achieved, and the relative error is within 1%.

The PSD of the vehicle response at m_s is calculated using the parameters in Table 1 as shown in Figure 11.

The kurtosis of the non-Gaussian vehicle response is calculated and compared with the kurtosis of the Gaussian vehicle response × AMS. The result is shown in Figure 12. From Figure 12, we can see a good match between these two kurtoses, showing that the AMS for both input road profile and vehicle response is the same. The kurtosis of vehicle response is about the same as the input road profile. This is predictable because, with a slowly varying AMS, the response under a non-Gaussian road profile is the same as the response under a Gaussian road profile, multiplied by the same AMS, hence resulting in the same kurtosis.

Finally, the FDS of vehicle response at m_s under non-Gaussian road profile excitation with different kurtosis and b values is simulated and compared with $Quot \times$ FDS under Gaussian road profile excitation as shown in Figure 13. The FDS is calculated at the maximum resonant frequency of the vehicle. From Figure 13, we can see that FDS increases as kurtosis and b value increase. A good match between FDS under a non-Gaussian road profile and $Quot \times$ FDS under a Gaussian road profile is obtained.

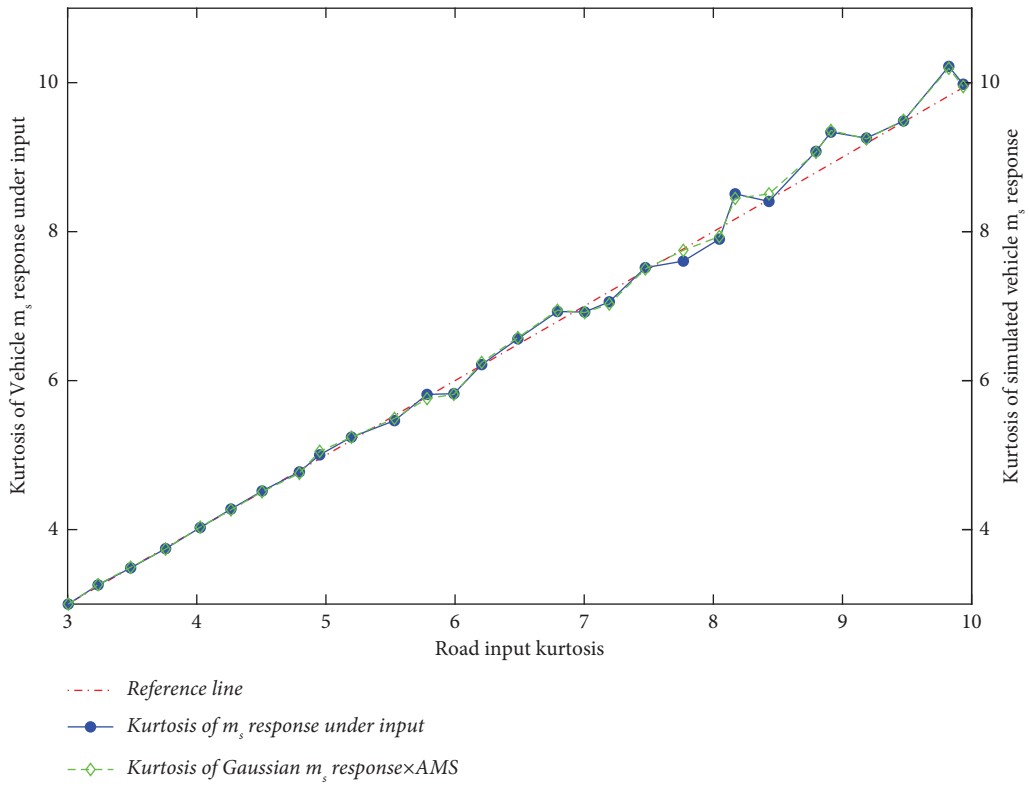

Figure 12: Kurtosis of non-Gaussian vehicle response and Gaussian vehicle response × AMS.

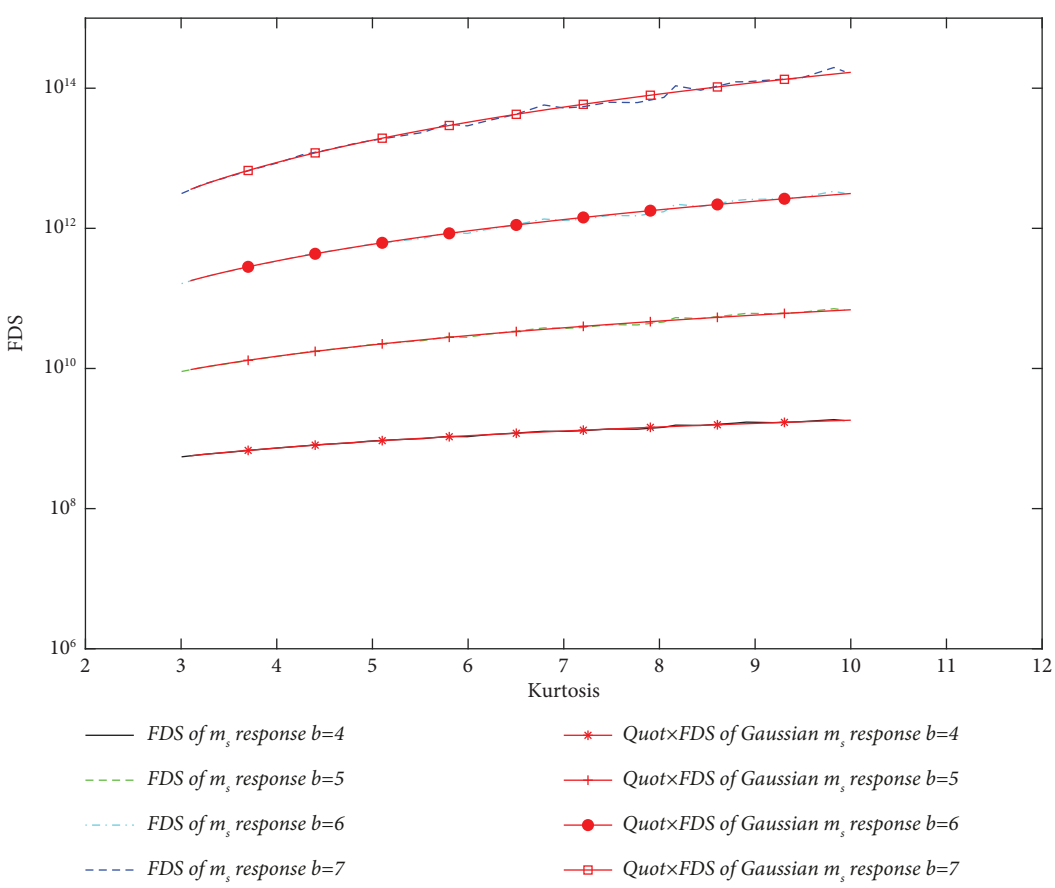

Figure 13: FDS of m_s response under non-Gaussian road profiles and *Quot* × FDS of m_s response under Gaussian road profile with different kurtosis and b values.

5. Conclusion

In this paper, the non-Gaussian road profile is simulated using the amplitude modulation method and used to study the vehicle vibration fatigue damage potential. Instead of using the iterative method, a closed-form formulation is presented to construct the AMS, with which the AMS parameter can be calculated directly from the kurtosis of a given non-Gaussian road profile. The theoretical relationship between the FDS of vehicle response under non-Gaussian and corresponding Gaussian road profiles is then formulated based on the AMS. Using the proposed method, a wide range of specified kurtosis of road profile is achieved. Given kurtosis and fatigue exponent b value, the extra fatigue damage caused by non-Gaussian road profile can be derived easily from the corresponding Gaussian road profile without calculating the vehicle response, which lays the foundation for a significantly simplified and more accurate fatigue test of vehicle vibration under non-Gaussian road profile. Although only the ISO-A pavement is simulated, the proposed method also applies to other types of pavement.

Data Availability

The data used to support the findings of this study are available from the corresponding author upon request.

Conflicts of Interest

The authors declare that there are no conflicts of interest.

Acknowledgments

This study was partially supported by the National Natural Science Foundation of China (Grant no. 52102443) and the Postgraduate Research and Practice Innovation Program of Yancheng Institute of Technology (Grant no. 1142247).

References

[1] Iso 8608, *Mechanical Vibration- Road Surface Profiles-Reporting of Measured Data*, International Organization for Standardization, ISO, Geneva Switzerland, 2016.

[2] P. Wolfsteiner and W. Breuer, "Fatigue assessment of vibrating rail vehicle bogie components under non-Gaussian random excitations using power spectral densities," *Journal of Sound and Vibration*, vol. 332, no. 22, pp. 5867–5882, 2013.

[3] B. Bruscella, V. Rouillard, and M. Sek, "Analysis of road surface profiles," *Journal of Transportation Engineering*, vol. 125, no. 1, pp. 55–59, 1999.

[4] V. Rouillard, M. A. Sek, and T. Perry, "Analysis and simulation of road profiles," *Journal of Transportation Engineering*, vol. 122, no. 3, pp. 241–245, 1996.

[5] V. Rouillard, "On the non-Gaussian nature of random vehicle vibrations," in *Proceedings of the World Congress on Engineering*, pp. 1219–1224, London, UK, July 2007.

[6] R. Zheng, C. Guo∗∗, and C. Huaihai, "Stationary non-Gaussian random vibration control: a review," *Chinese Journal of Aeronautics*, vol. 34, no. 1, pp. 350–363, 2021.

[7] D. Smallwood, "Vibration with non-Gaussian noise," *Journal of the IEST*, vol. 52, no. 2, pp. 13–30, 2009.

[8] S. Cui, R. Geng, C. Wang, and C. Cheng, "Study of the amplitude modulation method for kurtosis control purposes," *Mechanical Systems and Signal Processing*, vol. 179, Article ID 109399, 2022.

[9] F. Xu, C. Li, T. Jiang, and K. Ahlin, "Synthesis of running RMS-induced non-Gaussian random vibration based on Weibull distribution," *Journal of Vibroengineering*, vol. 17, no. 7, pp. 3662–3674, 2015.

[10] F. Xu, C. Li, and T. Jiang, "On the shaker simulation of wind-induced non-Gaussian random vibration," *Shock and Vibration*, vol. 2016, Article ID 5450865, 10 pages, 2016.

[11] A. Trapp, M. J. Makua, and P. Wolfsteiner, "Fatigue assessment of amplitude-modulated non-stationary random vibration loading," *Procedia Structural Integrity*, vol. 17, pp. 379–386, 2019.

[12] M. Troncossi and A. Rivola, "Response analysis of specimens excited with non-Gaussian acceleration profiles," in *Proceedings of ISMA2014*, pp. 799–808, Belgium, Europe, September 2014.

[13] S. A. Rizzi, A. Przekop, and T. L. Turner, "On the response of a nonlinear structure to high kurtosis non-Gaussian random loadings," in *Proceedings of the EURODYN2011-8th international conference on structural dynamics*, Hampton, VI, USA, July 2011.

[14] F. Kihm, N. S. Ferguson, and J. Antoni, "Fatigue life from kurtosis controlled excitations," *Procedia Engineering*, vol. 133, pp. 698–713, 2015.

[15] F. Kihm, S. Rizzi, N. Ferguson, and A. Halfpenny, "Understanding how kurtosis is transferred from input acceleration to stress response and it's influence on fatigue life," 2013, https://www.researchgate.net/publication/299447929_Understanding_how_kurtosis_is_transferred_from_input_acceleration_to_stress_response_and_it's_influence_on_fatigue_life.

[16] C. Braccesi, F. Cianetti, M. Palmieri, and G. Zucca, "The importance of dynamic behaviour of vibrating systems on the response in case of non-Gaussian random excitations," *Procedia Structural Integrity*, vol. 12, pp. 224–238, 2018.

[17] L. Capponi, M. Česnik, J. Slavič, F. Cianetti, and M. Boltežar, "Non-stationarity index in vibration fatigue: theoretical and experimental research," *International Journal of Fatigue*, vol. 104, pp. 221–230, 2017.

[18] W. Lei, Y. Jiang, X. Zeng, and Z. Fan, "Research on the transmission law of kurtosis of SDOF system under non-stationary and non-Gaussian random excitations," *Mechanical Systems and Signal Processing*, vol. 165, Article ID 108292, 2022.

[19] B. Cornelis, A. Steinwolf, M. Troncossi, and A. Rivola, "Shaker testing simulation of non-Gaussian random excitations with the fatigue damage spectrum as a criterion of mission signal synthesis," in *Proceedings of the International Conference on Engineering Vibration*, pp. 7–10, Slovenia, Europe, September 2015.

[20] A. J. D. Nanthakumar, K. Jariwala, K. Harshit, S. Yokeshwaran, and S. Madhankumar, "Classification of road profile using golden car parameters for quarter car model," in *Proceedings of the Advances in Design and Thermal Systems: Select Proceedings of ETDMMT 2020*, pp. 341–347, Springer, Singapore, March 2021.

[21] Iso 18431-4:2007, *Mechanical Vibration and Shock- Signal Processing- Part 4: Shock-Response Spectrum Analysis*,

International Organization for Standardization, ISO, Geneva Switzerland, 2007.

[22] H. A. Gaberson, "Shock severity estimation," *Sound and Vibration*, vol. 46, no. 1, pp. 12–20, 2012.

[23] G. R. Henderson and A. G. Piersol, "Fatigue damage related descriptor for random vibration test environments," *Sound and Vibration*, vol. 29, no. 10, pp. 20–25, 1995.

[24] A. Angeli, B. Cornelis, and M. Troncossi, "Synthesis of Sine-on-Random vibration profiles for accelerated life tests based on fatigue damage spectrum equivalence," *Mechanical Systems and Signal Processing*, vol. 103, pp. 340–351, 2018.